Minerals Engineering 82 (2015) 2–13

Contents lists available at ScienceDirect

Minerals Engineering

journal homepage: www.elsevier.com/locate/mineng

Semi-automated iron ore characterisation based on optical microscope analysis: Quartz/resin classification

I.D. Delbem, R. Galéry *, P.R.G. Brandão, A.E.C. Peres

Department of Mining Engineering, Universidade Federal de Minas Gerais, Av. Antonio Carlos 6627, Campus Pampulha, Escola de Engenharia, Bloco II s/4236, CEP 31.270-901 Belo Horizonte, MG, Brazil

ARTICLE INFO

Article history:
Received 30 December 2014
Revised 21 July 2015
Accepted 22 July 2015
Available online 24 August 2015

Keywords:
Iron ore characterisation
Liberation analysis
Optical microscopy

ABSTRACT

The present study focused on overcoming the primary problem faced by any quantitative mineralogical study involving iron ore characterisation using a reflected light optical microscope; distinguishing the quartz mineral from the epoxy resin in digital images taken from mounted polished sections. Difficulties arise in this case because both phases reflect in the same colour intensity range. To overcome this problem, a digital image analysis system denominated Opt_{-Lib} was developed. In order to evaluate the system responsivity, a characterisation study and modal and liberation analyses were performed using typical Brazilian iron ore containing quartz and the main iron oxide/hydroxide minerals: magnetite, hematite, and goethite. For the system performance evaluation, these results were compared with those generated by the scanning electron microscopy (SEM)-based Mineral Liberation Analyzer for the same sample. The results show that the main advantage of the Opt_{-Lib} system over the SEM-based system is that it facilitates differentiation, classification, and quantification of not only the quartz mineral, but also the iron oxide/hydroxide minerals within the sample, thus providing a more precise qualitative response.

1. Introduction

Consideration of mineral resource supply processes is the basis of any mining project evaluation. The specifics of mineral resource supply processes involve considerable risk; therefore, mineral characterisation and liberation analyses are fundamental for defining appropriate ore resource models, mining methodologies, and the most feasible processing routes. These are the fundamental stages of the mineral resource supply process. The advancement of digital technology has enabled the development of many applications that aim to minimize the risks involved in making such assessments. Modern systems are being employed in many areas, ranging from the scaling and planning of mineral deposits to the design and operation of mineral processing plants. These systems adopt multidisciplinary approaches, the main objective of which is to minimize the uncertainties associated with resource economic assessment. Such assessments are conducted in order to classify given resources into economically feasible or unfeasible prospects.

The success of these studies is strongly dependent on the characterisation tools used. These tools, combined with analysis of traditional attributes such as content and metallurgical recovery, allow for a better understanding of the nature of a given mineral deposit. Properties related to descriptive and quantitative mineralogy (modal analysis), mineral liberation, and mineral associations influence not only processing methods, but also metallurgical recovery. Once the main ore properties that influence the processing methods are characterised for a given deposit, they in turn allow the major lithotypes that constitute the economic or mineable reserves to be defined in the mine planning stage. All these concepts and knowledge collectively are critical for optimization of the mine-to-mil process and now constitute the field of study known as geometallurgy (Dunham and Vann, 2007; Lin et al., 2013).

The success of a geometallurgic study is completely based on precise characterisation of ore properties. Traditionally, mineralogical characterisation is performed using systems based on either a reflected light optical microscope (RLOM) or a scanning electron microscope (SEM). These studies require time and financial resources. Further, if they are based on a very small data sample, semi-quantitative results of dubious statistical precision are obtained.

In recent years, more advanced techniques have been made available. Powerful computers and RLOM- or SEM-based systems have been integrated with digital image analysis systems. A significant number of ore characterisation analysis methods have been

* Corresponding author.
E-mail address: rgalery@demin.ufmg.br (R. Galéry).

http://dx.doi.org/10.1016/j.mineng.2015.07.021
0892-6875/

proposed. Automated particle size measurement (Shutherland, 2007) and automated particle size distribution analyses (King, 1984) have been proposed as a means of controlling ore liberation and separation. It has also become evident that the analysis of mineral associations and precise studies of mineral liberation can only be conducted using imaging techniques (King, 1984; Donskoi et al., 2007). In the field of RLOM, a number of relevant contributions have been made (Poliakov and Donskoi, 2014; Donskoi et al., 2007, 2010, 2013a,b; Iglesias et al., 2011; Pirard et al., 2007; Pirard, 2004). As regards SEM based systems, three systems merit particular attention: *QEMSCAN* (Goodall et al., 2005), the Mineral Liberation Analyzer (*MLA*) system first introduced in 1997 (Gu and Napier-Munn, 1997), and more recently, the *LibMin* system (Delbem, 2010). The *MLA* system (Fandrich et al., 2007) and *QEMSCAN* combines images from a backscattered electron (BSE) detector with a mapping analysis via energy dispersive X-ray spectrometry (EDS). The *LibMin* system is similar to the *MLA* and *QEMSCAN*, with the disadvantage that is does not facilitate sample mapping via EDS.

Both RLOM- and SEM-based systems have certain advantages and disadvantages, which become evident in iron ore characterisation studies, as can be seen in Fig. 1.

For SEM-based systems, compositional information is obtained from the relationships between the number of produced BSE and the mean atomic number (MAN) of the sampled minerals (Chescoe and Goodhew, 1990). The BSE/MAN rate provides the contrast level in the generated digital image, as shown in Fig. 1a. EDS mapping can also provide compositional information. However, for iron ores, difficulties arise because of the similarities presented by hematite and magnetite as regards their mean atomic numbers and chemical compositions. Characterisation studies performed on iron ore sinter (Tonzetic and Dippenaar, 2011) using a QEMSCAN system confirm this assumption. The iron-ore-sinter characterisation results obtained in the above study exhibit large fluctuations in the obtained magnetite component values. This is thought to be the result of computer grey-scale drift, since there is a very fine distinction between hematite and magnetite grey-scale values. A similar result has also been reported (Donskoi et al., 2013b) for iron ore characterisation performed using the same SEM-based system. In other words, hematite and magnetite cannot be compositionally identified and classified as different mineral species using SEM-based systems. However, in RLOM-based systems, the iron oxide/hydroxide minerals (hematite, magnetite, and goethite) contrast and can be recognized as different mineral species, as depicted in Fig. 1b. Successful RLOM-based studies have already been reported (Iglesias et al., 2011; Donskoi et al., 2010). However, problems arise as regards discrimination between different phases, such as between minerals (quartz) or epoxy resin with similar reflectivities. Both reflect in the same range, restricting the application of RLOM to certain mineral systems (Launeau et al., 1994; Neumann and Stanley, 2008). In the field of RLOM, distinction between non-opaque minerals and epoxy resin has been an issue for many years. Discrimination between quartz and epoxy resin continues to pose the greatest difficulties.

As regards a geometallurgical approach, additional efforts must be made to successfully overcome the continuing dilemma of whether SEM- or RLOM-based systems should be used for iron ore characterisation. Improvement of the existing systems has become of paramount importance, along with the development of more sophisticated analytical systems for iron-ore microstructural (textural) characterisation.

In order to achieve these objectives, a digital image analysis system denominated Opt_{-Lib} was developed in this study. The approach used here focused on applying RLOM to iron ore mineralogical characterisation and liberation analysis. Since the terminology generally used in the field of liberation tends to be loose the following definitions will be used in the present paper:

> *degree of liberation:* fraction of a phase (by volume for particles, by area (areal) for sections, and by length for segments) present in liberated particles (or sections or segments), (Barbery, 1992).
> *liberation spectrum:* used to refer to the distribution of mineral composition (by volume, area or length) in a particle population (Schneider, 1995).

The Opt_{-Lib} system analyses acquired digital images for a given set of particle size classes, to allow the main iron ore mineral phases: quartz, goethite, hematite, and magnetite to be identified and classified. In this first stage, a developed sequence of techniques that allows quartz to be distinguished from resin is also applied. When the first stage is complete, the following sequence of tasks is performed for each particle size class: areal composition calculation; particle classification based on composition; evaluation of the free particle content in the population; and, finally, evaluation of relative liberation spectra.

2. Methodology

2.1. Sample preparation and instrumentation

An iron ore sample (itabirite) from the Brazilian Iron Quadrangle, specifically, from the Mariana, Minas Gerais, region, was selected for Opt_{-Lib} testing. The sample was first characterised using a Philips X-ray diffractometer (model PW1710) with a Cu Kα radiation crystal (scanning speed: 0.06° 2θ/s counting time, scanning interval: 4–90° 2θ). The mineral phases were identified by X-ray diffraction using the ICDD (International Centre for Diffraction

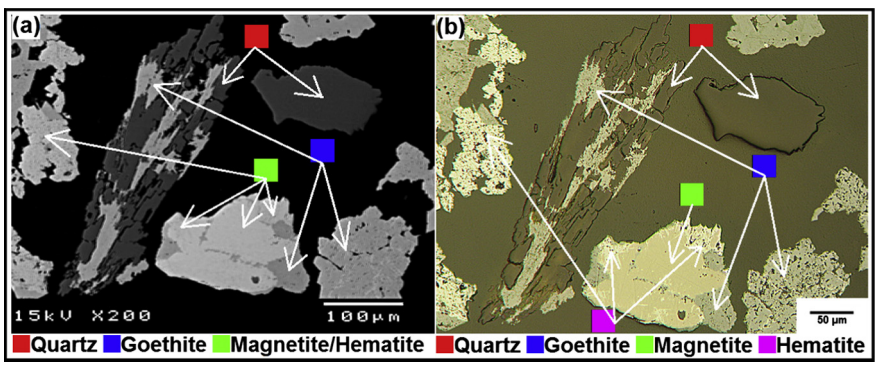

Fig. 1. Images sampled from the same area by different systems: (a) SEM; (b) RLOM.

Data) PDF-2, a collaborative product designed for inorganic materials analyses. For image acquisition, an adapted RLOM (Leitz/Leica, model: Orthoplan Pol) with a digital camera (Canon PowerShot S80) was used. The microscope was set to operate using polarised reflected light and the digital camera was set to capture 24-bit RGB images with a spatial resolution of 1600 × 1200 pixels.

The iron ore samples were classified by size, adopting $\sqrt{2}$ as the progressive sieve ratio. The particles of each size class were then mounted in polished sections. For the liberation analysis, size classes of 300–212, 212–150, and 150–106 μm, were prepared in a 25-mm-diameter epoxy resin mount. The preparation of the epoxy resin mounts included the careful addition and homogenisation of a high-viscosity epoxy resin to the original base resin. The objectives of this preparation process were:

- To reduce the mineral particle sedimentation rate. This enabled the resin hardening process to finish before the particles were completely deposited at the bottom of the mount. This procedure reduces problems related to particle preferred orientation and also neighbouring particles in close proximity to each other.
- To prevent particle pores from becoming filled with resin. This contributes to the identification of these structures in digital RLOM images.

The polishing process also followed the standard procedures necessary to preserve particle structure, minimize particle/resin topological problems, prevent particle detachment from the resin, and ensure that the surfaces of each mineral phase on the polished sections were completely uniform. The sample preparation methodology which best describes the required in this study, were:

- Samples mounting in epoxy resin: the mounting were assembled using a 25 × 25 mm cylinder. For each particle class size a mix prepared in a proportion, by weight, of 7:2:1:2 regarding respectively to epoxy resin, catalyzer, high viscosity copolymer, and mineral particles, were prepared. After assembling, the mounting set were submitted to vacuum in a vacuum chamber to remove any air bubble formed during the mixing step.
- Roughing and polishing: after hardening, the mounts were submitted to a first course roughing stage to take off the first particles layer. This process is important to reduce dense phases preferential orientation. The roughing stage is followed by the graining stage using a sequence of sandpaper mesh sizes: 240, 320, 400, 600 and 800. Later on the mounting sections were submitted to a polishing stage using a sequence polishing diamond pastes whose mesh sizes were respectively, 15 μm, 9 μm, 6 μm, 3 μm, 1 μm and 0.25 μm.

For roughing and polishing it was used a Buehler polishing system model Minimet 1000 whose polishing parameters are presented in Table 1.

It is worth to point out that the polishing procedures are critical to obtain good quality RLOM digital images. The accuracy of the image analysis results will strongly rely on the sampling preparation procedures.

Table 1
Polishing parameters.

Polishing time (min)	Speed (rpm)	Force (N)	Diamond paste (μm)
25	25	25	15
25	25	25	9
25	20	20	6
30	20	20	3
30	20	15	1
20	20	10	0.25

In order to validate the results obtained using the *Opt*$_{-Lib}$ system, a comparative study was conducted using the same polished sections. These samples were also submitted for analysis in a MLA system, the MLA 650 (SEM-FEG-Quanta 650; FEI), which was supplemented with an EDS (Quantax; Bruker).

2.2. Image acquisition and pre-processing

Before the digital image acquisition and after mounting of the polished sections of each size class on the microscope stage, the RLOM was fully adjusted and calibrated so that all of the sampled digital images exhibited the same colour intensity characteristics for all samples. This means that, for a specific phase, the colour intensity range that characterised this phase was present in the same histogram region for all sampled images. This procedure allows an optimal system configuration for the processing of all images of a given polished section to be defined. In order to illustrate this procedure, Fig. 2 shows two digital images and their respective histograms, which were obtained for different areas of the same polished section for the 150–106-μm size class.

It is also important to select for each particle size class, the correct magnifying lens that will keep the same approximate number of particles in the sampled view area, not considering particles that touch the image borders. In Fig. 2, the number of particles in the viewing area was set to approximately 6. After digital image acquisition, the obtained image sets were submitted to a pre-processing stage consisting of: background correction, sharpening, delineation, and smoothing. All these pre-processing techniques have already been addressed in previous works (Delbem, 2014).

3. Results and discussion

The *Opt*$_{-Lib}$ system was developed to quantify mineral phases (modal analysis) and to conduct liberation studies of phases of interest (iron-bearing minerals) from gangue minerals (quartz). This system is based on a routine that was developed to classify and distinguish quartz from resin in digital images of polished sections obtained using a RLOM. The iron ore sample information used in the present study and, also, the main techniques implemented in the *Opt*$_{-Lib}$ system are described below.

3.1. Sample characterisation

The iron ore sample from the Brazilian Iron Quadrangle was subjected to X-ray diffraction analysis. The results show that the sample was primarily composed of quartz (αSiO_2), goethite ($FeO{\cdot}OH$), hematite (Fe_2O_3), and magnetite ($Fe_2O_3{\cdot}FeO$).

3.2. Automated mineral phase segmentation procedure – identification of cluster dissimilarities

Difficulties in identifying and classifying a finite set of entities (grey-scale intensities) into groups of similar objects (clusters or mineral phases) are often encountered in many different research fields. Here, the choice of grey-scale images for this process merits explanation. Firstly, the availability of very sensitive digital cameras allows RGB thresholding to be performed. Also, the continuous increase in computer processing power has facilitated the development of complex image-analysis routines for mineral discrimination based on sample reflectivity and texture. Thus, dynamic thresholding is also possible (Donskoi et al., 2013a; Poliakov and Donskoi, 2014). It is a fact that, for the majority of iron ore minerals, reflectivity differences there exist and can be observed on the grey-scale level. Therefore, grey-scale images can also be considered when developing mineral discrimination techniques.

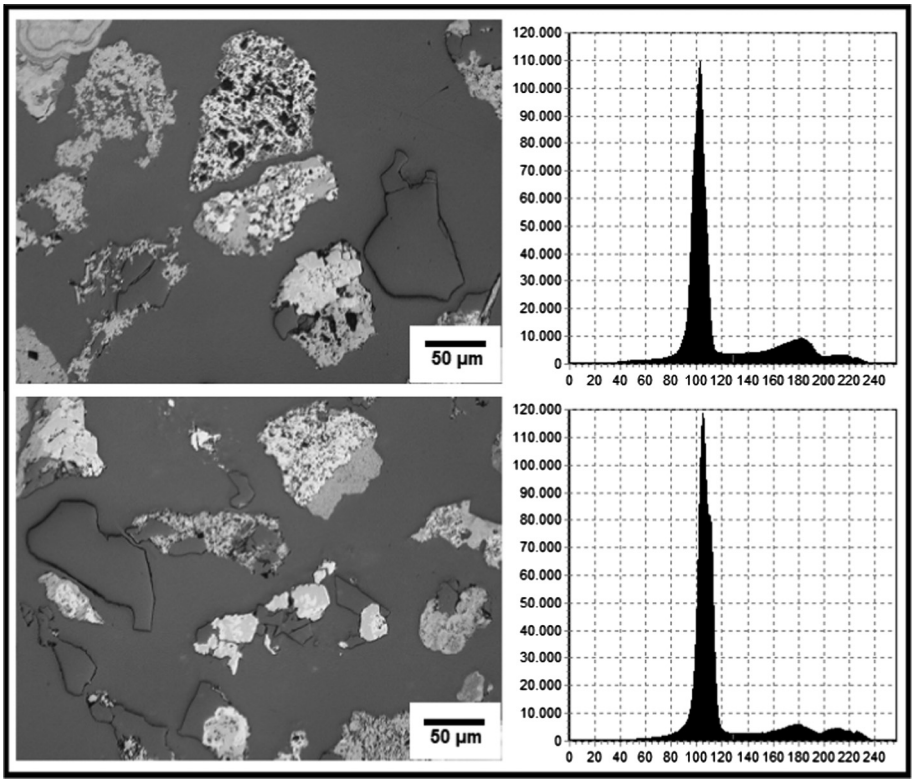

Fig. 2. Particle images and respective image histograms taken from different areas of the same polished section for the 150–106-μm size class.

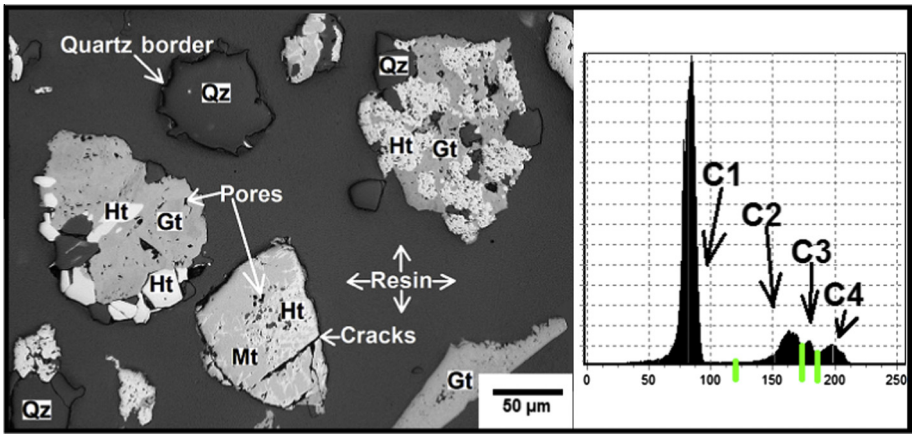

Fig. 3. RLOM image taken from iron ore sample containing quartz (Qz), goethite (Gt), magnetite (Mt), and hematite (Ht).

Thus, the developed system for mineral discrimination is based on a one-channel histogram analysis of digital images. The histogram of a digital image with L total possible intensity levels in the [0, L] range is defined as the discrete function

$$h(i_k) = n_k, \tag{1}$$

where i_k is the k_{th} intensity level in the [0, L] interval and n_k is the number of pixels in the image with i_k. The L value is equal to 255 for 8-bit images.

The developed routine searches for the optimum partitioning of a set of finite entities (intensities) into groups of "similar" objects, referred to as clusters here. The methodology is an approximation of the optimum partitioning via global optimization of a selection of "cluster seed points" (Diday and Moreau, 1984), and adopts the following parameters:

$I = \{I_K | k = 0 \ldots L\}$, the set of grey-level intensities to be partitioned;
$D = \{d_{kl} | k, l = 0 \ldots L\}$, the set of dissimilarities, where $d_{kl} = d(I_k, I_l)$ between all pairs of grey-level intensities;
$P_M = (C_1 \ldots C_M)$, the partition of I into M clusters;
π_M defined as the set of all possible P_M.

Using the above notation, the optimal partition set (OPS) problem can be verbally expressed as:

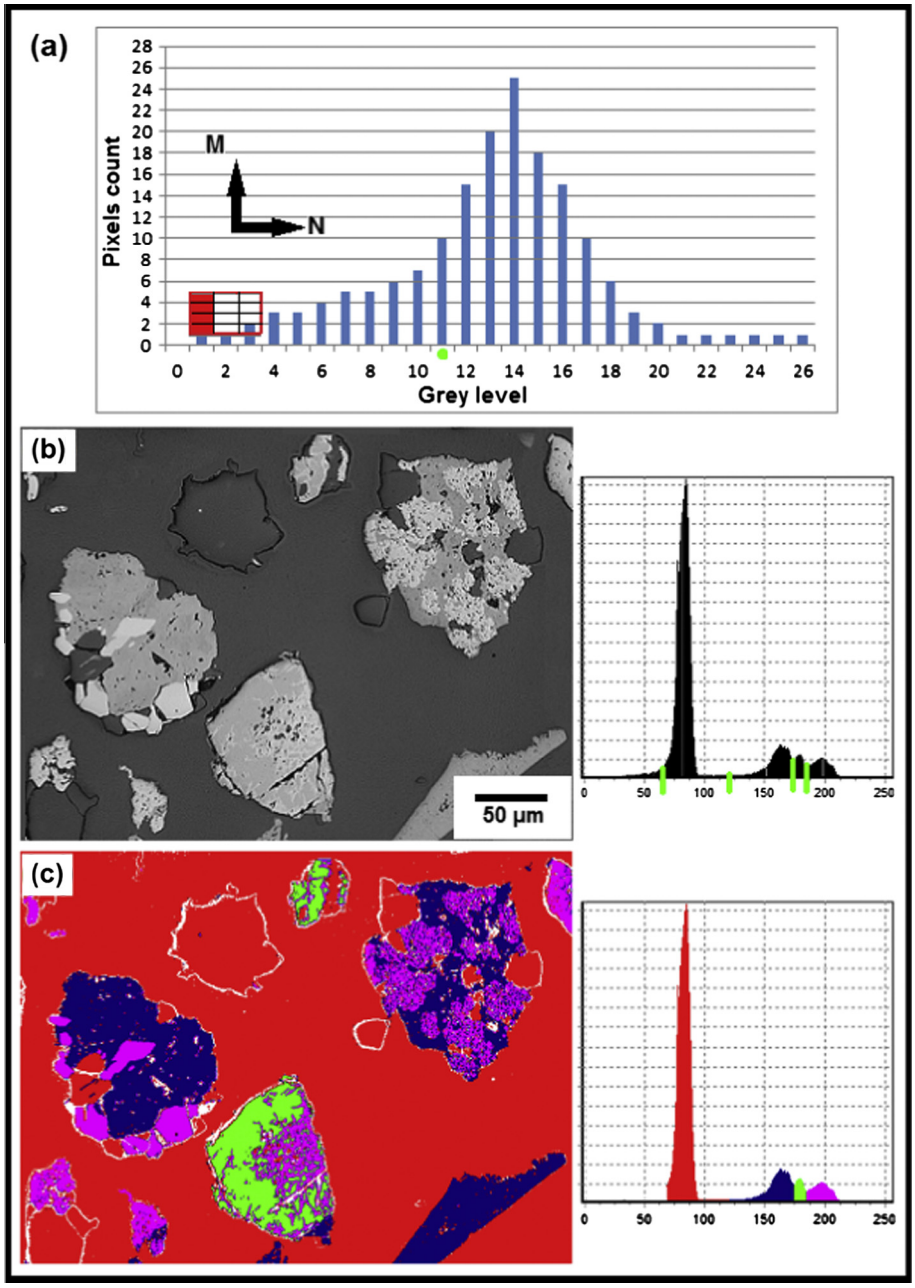

Fig. 4. (a) Graphical representation of the $N \times M$ mask recursively applied for boundary definition; (b) RLOM image with sub-clusters exhibiting defined borders, pores, and cracks; (c) image (b) with pseudo-colours attributed to each of the clusters: borders, pores, and cracks (white), quartz/resin (red), goethite (blue), magnetite (green), and hematite (magenta). (For interpretation of the references to colour in this figure legend, the reader is referred to the web version of this article.)

(OPS) Find a partition, $P_M \in \pi_M$, that provides the most homogenous (discriminative) classification of the set of grey-level intensities, I, as expressed in terms of the dissimilarities, D.

Additional parameters are also defined:

$D(C_j) = \max d_{kl}$, $(I_k, I_l \in C_j)$, the diameter of cluster C_j;
$r(C_i, C_j) = \min d_{kl}$, $(I_k \in C_i; I_j \in C_j)$, the distinction between C_i and C_j;
$s(C_j) = \min d_{kl}$, $(I_k \in C_j; I_l \notin C_j)$, the split of cluster C_j.

The results obtained through application of the clustering algorithm are presented in Fig. 3, in which four distinct regions are defined in the histogram. The clustering procedures are induced by the $s(C_j)$ seed points (in green). From left to right, C_2, C_3, and C_4 represent, respectively, goethite, magnetite, and hematite; the three "homogeneous" clusters on the grey-level scale.

The grey-scale region, represented by the leftmost cluster in the histogram includes other important structures besides quartz and epoxy resin, such as particle edges, pores, and cracks. Distinguishing these structures from epoxy resin can be very difficult or even impossible. The main concept of the developed method for discriminating between such structures was, in fact, fully based on observations obtained from analysis of the C_1 cluster. The frequencies of structures such as particle edges, pores, and cracks are represented by the lower intensity values on the histogram to the first peak of the maximum frequency observed in the range of the C_1 cluster. These structures can occasionally appear as an additional

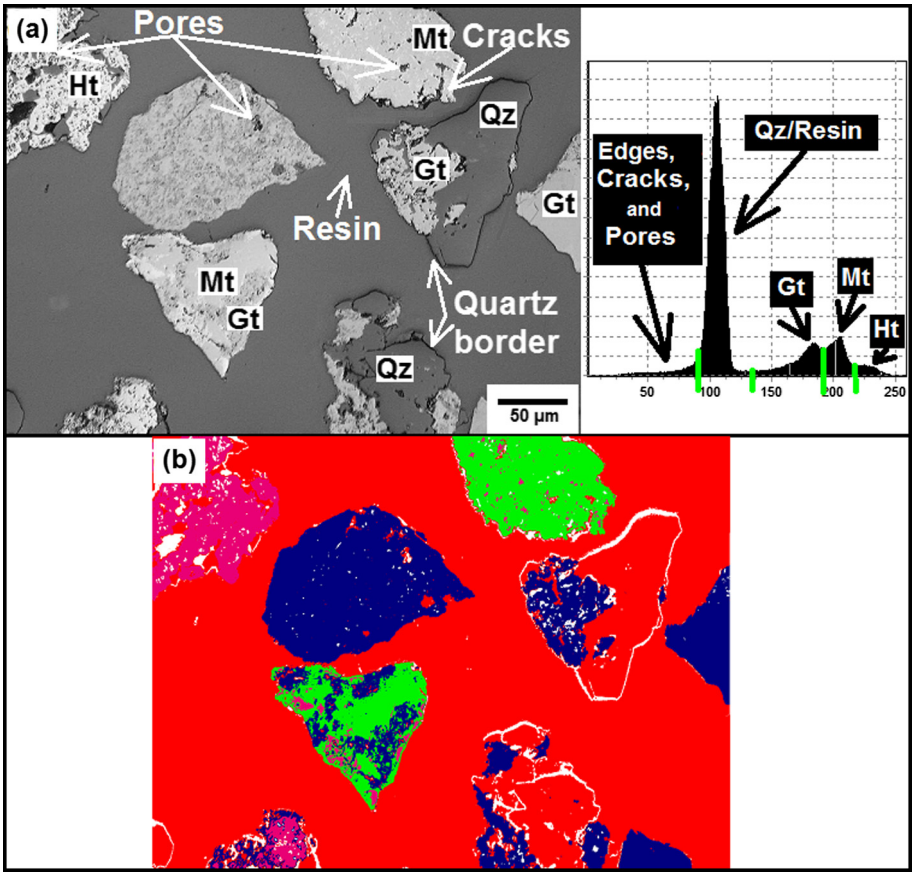

Fig. 5. (a) RLOM digital image from an iron ore sample showing the mineral phases containing quartz (Qz), goethite (Gt), magnetite (Mt), and hematite (Ht); (b) image (a) after the segmentation procedure described in Sections 3.2 and 3.3.

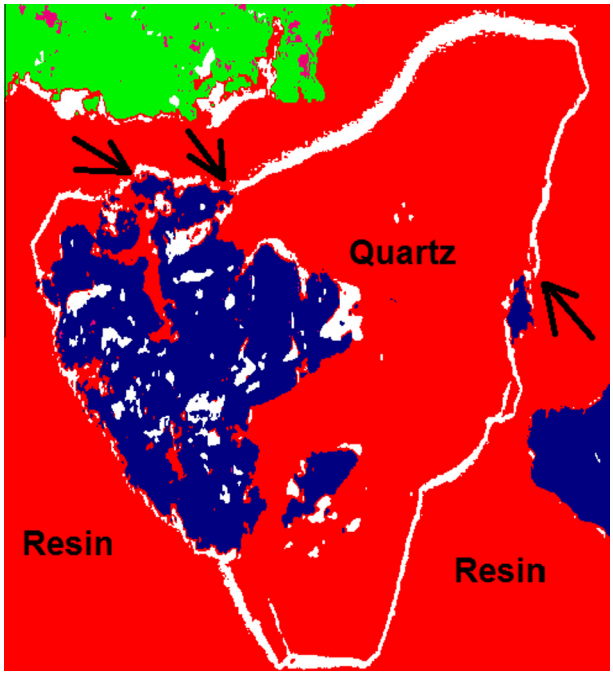

Fig. 6. Selected section of Fig. 5b showing quartz border discontinuities (arrows) after the segmentation process.

cluster (labelled C_0) on the histogram; however, this rarely occurs. In the additional cluster case, the extra cluster that represents these structures is indicated by intensities beginning at the lowest values and gradually increasing in value until an "inflection" point is reached. From this inflection point, the intensity increases rapidly, until the maximum frequency value on the histogram is reached.

Here, the C_1 cluster was found to contain distinct particle structures that can be partitioned. One sub-cluster is composed of intensities ranging from the lower values to the "inflection" point, and indicates particle structures such as borders, pores, and cracks. The second sub-cluster ranges from the "inflection" point to the higher limit of the C_1 cluster and is the quartz/epoxy resin sub-cluster. In order to identify the C_1 "inflection" point, which is the seed point (or threshold boundary) for the two-sub-cluster partition, a specific procedure was adopted.

3.3. Sub-cluster dissimilarity identification procedures

According to the statements from Section 3.2, it is possible to fully identify certain particle structures, such as borders, pores, and cracks. It is also suggested that the dissimilarity approach cannot be used to completely overcome clustering problems when one particular intensity (epoxy or quartz) dominates the very-high-frequency range of the histogram. This is the fundamental problem faced by many mineralogists when attempting to discriminate between non-opaque minerals, such as quartz, and epoxy. Even when the mineral borders separating quartz from epoxy are reasonably well visible, as in Fig. 3a, those structures cannot be segregated through thresholding. In order to overcome this problem, the following procedure was adopted.

Let ω be a finite set and H a set of all parts (called levels). H is a hierarchy in ω if:

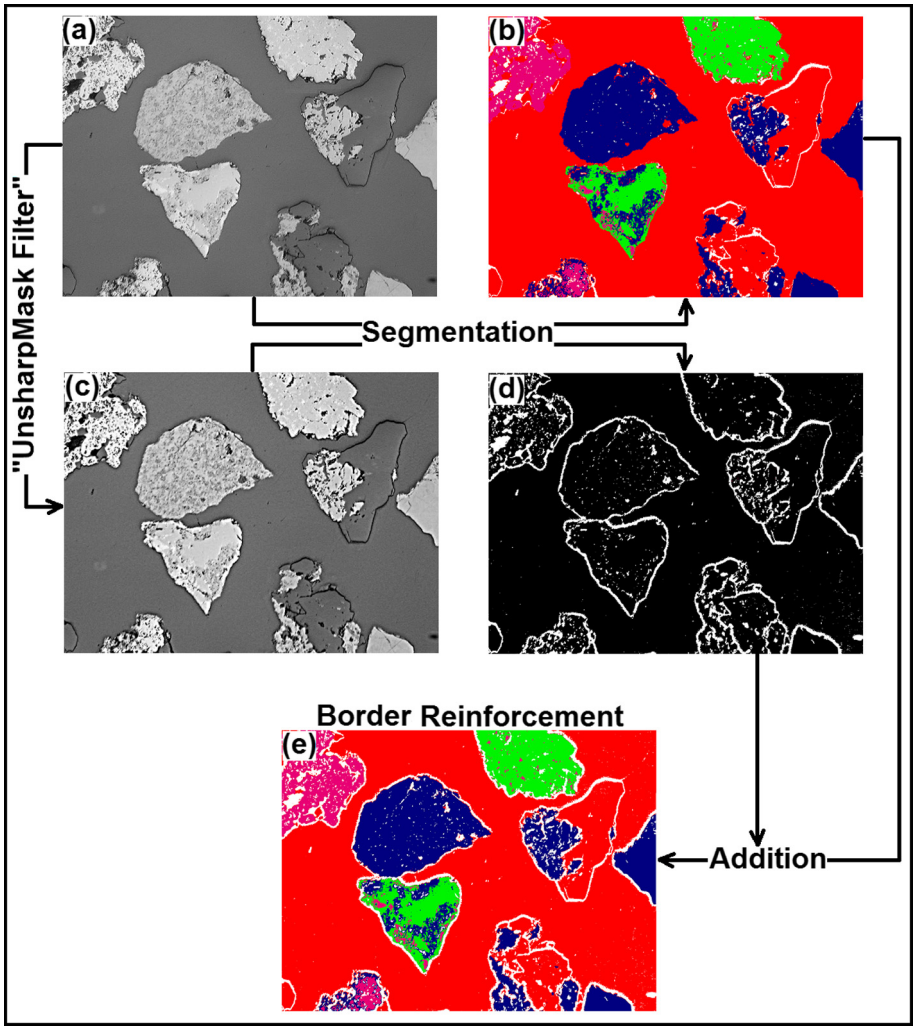

Fig. 7. (a) Pre-processed digital image from RLOM; (b) segmented image (clustering and sub-clustering); (c) image after "UnsharpMask" filter application; (d) image (c) after segmentation resulting in the enhancing of the borders, pores and cracks; (e) image produced by addition of images (b) and (d).

(1) $\omega \in H$ {i.e., the highest level contains all the individuals};
(2) $\forall w \in \omega{:}\{\omega\} \in H$ (terminal points).

An indexed hierarchy is a couple (H, f) in which H is a hierarchy and f is an application of H in $\Re$ such that:

(1) $\forall\ h, h' \in H$: $\delta(h, h') \geqslant 0$ (positiveness);
(2) $\forall\ f(h), f(h')$: $\delta(f(h), f(h')) \geqslant 0$ (positiveness);
(3) $\forall\ \delta(h, h') = N$: $\delta(f(h), f(h')) > M$ (terminal condition, seed point definition).

An implementation of the procedures described above is graphically presented in Fig. 4a. A $N \times M$ mask must be recursively applied until the terminal condition is reached, where the seed (threshold) point is defined. The value of N is given in units of intensity, while the value of M is given in units of frequency. M is evaluated at each positive displacement until the terminal condition is reached. In this example, an intensity value $N = 11$ was found as the seed point (in green). Fig. 4b presents a RLOM digital image taken from an iron ore sample containing quartz (Qz), goethite (Gt), magnetite (Mt), and hematite (Ht). The image histogram presents the seed point that defines the two additional sub-clusters, with the leftmost cluster representing the borders, pores, and cracks.

In Fig. 4b, pseudo-colours have been attributed to each distinct cluster. It can be seen that the clustering and sub-clustering segmentation routines described above have allowed very important structures to be defined (particle edges, pores, and cracks, indicated by white), along with the main minerals: goethite (blue), magnetite (green), and hematite (magenta). However, it can be clearly seen from these results that quartz and resin (in red) discrimination remains an unsolved problem.

3.4. Quartz-epoxy resin classification

Clustering processes fail to identify, classify, and discriminate between quartz grains and epoxy resin in RLOM digital images. This is due to the similarities in the colour intensities exhibited by both phases. Therefore, to overcome these problems, it was necessary to develop very specific techniques in this study. These techniques must be intensively applied in two stages. The first stage constitutes the sample preparation methodology, incorporating careful mounting and polishing of the sample sections as described in Section 2 (Delbem, 2014). The second stage consists of the computational work necessary to enhance the particle borders, primarily emphasizing the borders around quartz. Fig. 5a is a RLOM digital image taken from the iron ore sample (itabirite) containing quartz (Qz), goethite (Gt), magnetite (Mt), and hematite

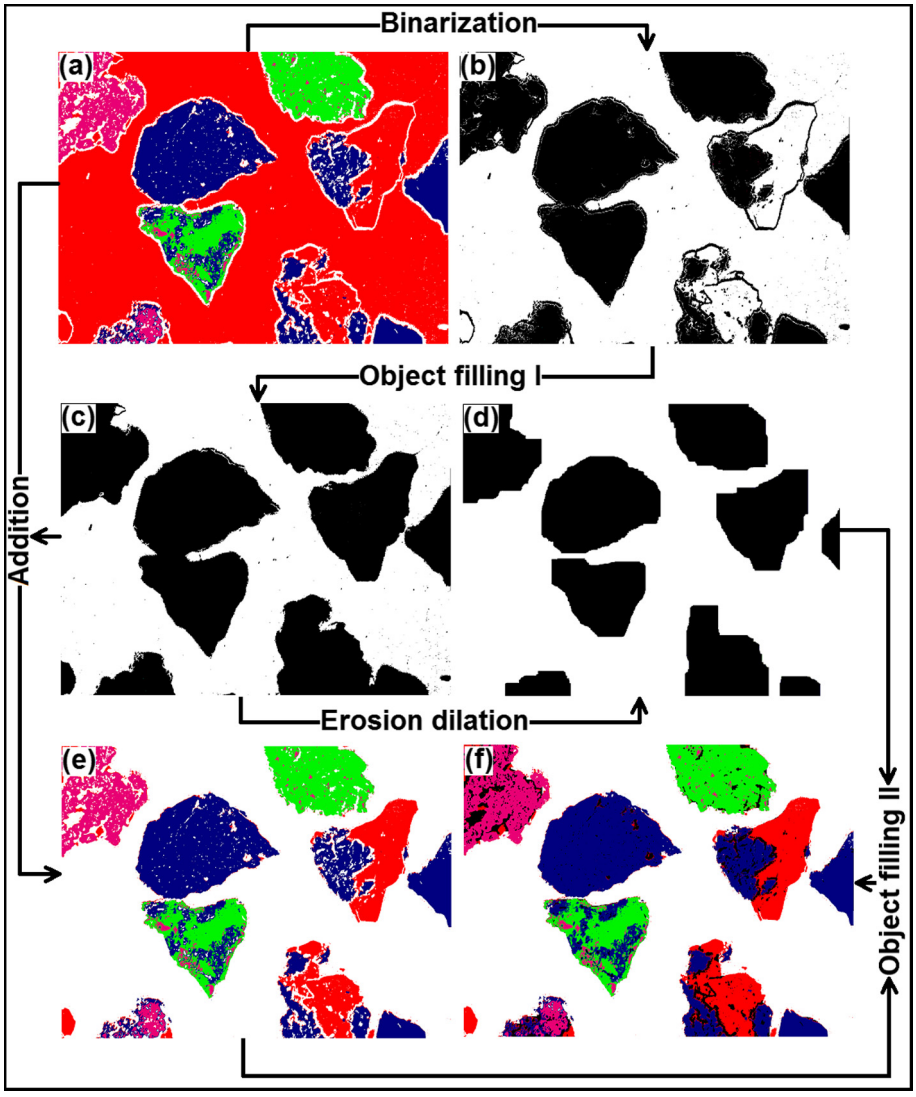

Fig. 8. (a) Image with quartz border reinforcement; (b) segmented input image (binarisation); (c) filling process applied to image (b); (d) image (c) following erosion–dilation process; (e) images (a) + (c); (f) logic operation applied to images (d) and (e) to fill and enhance particle pores and cracks.

(Ht). Fig. 5b shows the input image after application of the segmentation procedures described in Sections 3.2 and 3.3.

In Fig. 5a, the quartz borders consist of a low intensity line resulting from the association of two distinct effects: the first is related to a slightly topological difference that is exhibited by quartz in relation to resin; the second is associated with the well-known Becke line effect (Wahlstrom, 1969), which is usually observed in transmitted light optical microscopy (TLOM) images. Nevertheless, this effect can also be observed less intensively in RLOM images. The developed segmentation routine also utilises the Becke line effect for the classification and identification of quartz and for discrimination between quartz and resin. The developed procedure considers this lower intensity line to be the boundary between the two materials and thereby discriminates between the quartz and resin. To successfully distinguish quartz from epoxy resin, the borders around the quartz must be continuous after segmentation (sub-clusters processing). However, segmentation processes alone cannot guarantee completely continuous quartz borders. Fig. 6 shows a selected portion of image Fig. 5b, which clearly demonstrates that discontinuity problems still exist at the quartz borders.

In order to enhance the quartz borders, the "UnsharpMask" filter (Gonzalez and Woods, 2008) was selected and carefully configured for application to this specific case. The filter allows the input image, $f(x, y)$, to be obtained from a blurred image, $\bar{f}(x, y)$. In the sequence, an unsharpened mask, $g_{mask}(x, y)$, is obtained, according to the expression

$$g_{mask}(x,y) = f(x,y) - \bar{f}(x,y), \tag{2}$$

To obtain the enhanced image, $g(x, y)$, a weighted proportion, k ($k \geqslant 1$), of $g_{mask}(x, y)$ is added to $f(x, y)$, such that

$$g(x,y) = f(x,y) + k^* g_{mask}(x,y), \tag{3}$$

For border enhancement, the "UnsharpMask" filter must be correctly configured. Adjustments of the blur filter and k must allow dark pixels (pixel halos) to be produced around all objects in $g(x, y)$. This procedure is very important, because the resultant image ensures the continuity of the quartz borders. The quartz border enhancement process is sequentially presented in Fig. 7.

Fig. 7e is the final result of the quartz border reinforcement procedures. From this point, the process to discriminate between the

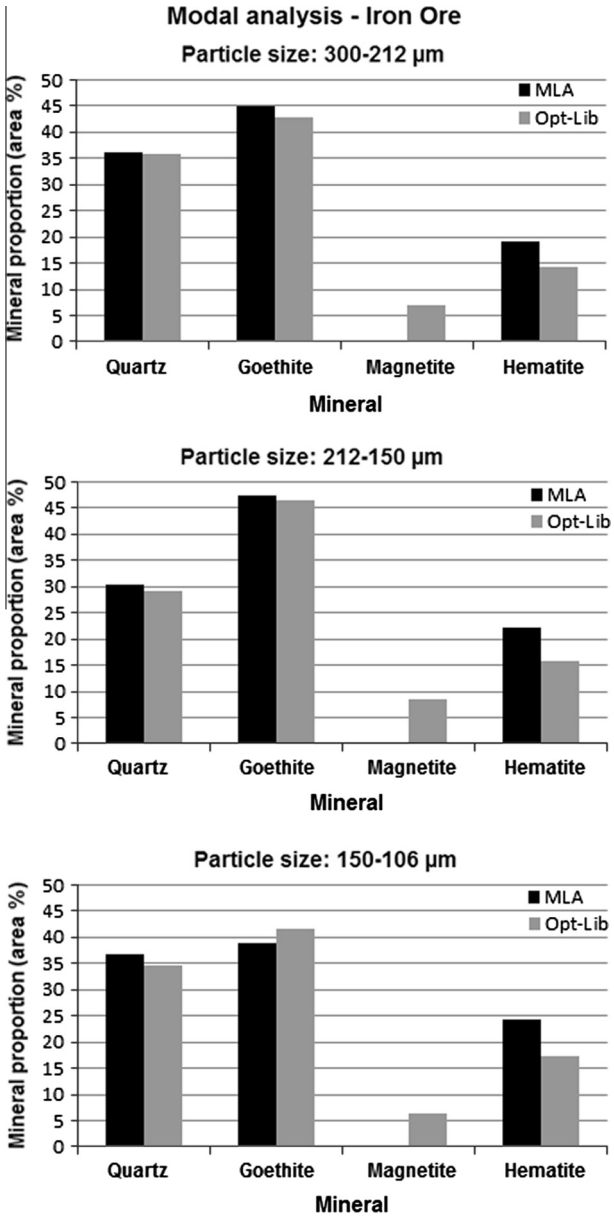

Fig. 9. *Opt*$_{Lib}$ and *MLA* mineral phase quantification for the size classes: 300–212, 212–150, and 150–106 µm.

quartz and the resin can be conducted. This process is sequentially presented in Fig. 8.

Beginning with the input image resulting from the border reinforcement process (Fig. 8a), an "auxiliary image" is obtained (Fig. 8b). In this auxiliary image, all pixels representing quartz and resin are set to white, while all other pixels are set to black. In the next step, all particles in the auxiliary image (Fig. 8b) are subjected to an inner filling process (Fig. 8c), and the inner pixels of all particles are set to black. To distinguish the resin from the quartz, the primary image (Fig. 8a) must be added to the auxiliary image (Fig. 8c), resulting in the image depicted in Fig. 8e. In the sequence, the auxiliary image (Fig. 8c) is subjected to an erosion and dilatation procedure, the results of which are shown in Fig. 8d. This image is used as a "background" for the particles in the image obtained through the addition process (Fig. 8e). The complete and final processing data are shown in Fig. 8f.

Regarding these procedures, it can be observed that the particle borders represented by the white pixels in Fig. 8a simply vanish after the addition process (Fig. 8e). This is very convenient, because particles that are in contact with each other are de-agglomerated and preserved as distinct objects. After the addition process (Fig. 8e), it can be seen that internal particle structures such as cracks and pores are still preserved (in white). Here, many different problems that impact the ore characterisation and liberation analysis process can arise. For instance, considering a crack along a single particle, this single particle can be sectioned as two different particles. Further, image processing operations such as erosion and dilation can be applied in this specific case to assure particle integrity. Usually, this technique is applied to binary images such as the image shown in Fig. 8c. In this case, the erosion procedure can be applied several times to the infilled "auxiliary image" (Fig. 8c) to guarantee object separation. Dilation must be also applied to compensate for the erosion; however, the dilation technique has slightly less iterations than the erosion process. The erosion–dilation procedures do not affect the particle structure, and they are exclusively applied to ensure that particle pores and cracks are preserved and can be distinguished from epoxy resin.

The resultant segmented image (Fig. 8f) can be subjected to the typical post-processing routines: elimination of spurious artefacts (very small particles or fragments that do not match the particle size class under investigation) and elimination of particles that touch the image borders. From this point, the techniques used within the *Opt*$_{Lib}$ system can be applied in order to classify and quantify the mineral phases and, also, to evaluate the mineral liberation spectrum.

3.5. *Opt*$_{Lib}$ performance evaluation

To evaluate the *Opt*$_{Lib}$ system performance, an iron ore sample from the Brazilian Iron Quadrangle was selected. The polished sections were first subjected to *Opt*$_{Lib}$ system analysis, followed by *MLA* system analysis. The main objective of the present study was to compare both results to evaluate the performance of the *Opt*$_{Lib}$ system. The *MLA* system was chosen for this comparative evaluation because it is a very powerful and sophisticated system that is dedicated to liberation analysis.

3.5.1. Iron ore mineral characterisation and quantification – modal analysis

X-ray diffraction data indicated the presence of the following minerals in the iron ore sample: quartz, goethite, hematite, and

Table 2
Mineral phase quantification performed using the *Opt*$_{Lib}$ and *MLA* for the size classes: 300–212, 212–150, and 150–106 µm.

Particle size (µm)	System	No. of particles	Quartz (area %)	Goethite (area %)	Hematite (area %)	Magnetite (area %)
[300–212]	MLA	1180	36.1	44.9	19	0
	OptLib	1250	35.9	43	14.2	6.9
[212–150]	MLA	1100	30.3	47.5	22.2	0
	OptLib	1150	29.2	46.4	15.9	8.6
[150–106]	MLA	1180	36.8	38.8	24.4	0
	OptLib	1250	34.7	41.6	17.2	6.5

Table 3
Particle distributions by areal composition class. Data from *MLA* and *Opt*$_{-Lib}$ for the size classes: 300–212, 212–150, and 150–106 μm (the distribution for each size class is normalized to 100%).

Particle size (μm)	System	No. of particles	Distribution by composition class											
			0%	0% < X < 10%	10% < X < 20%	20% < X < 30%	30% < X < 40%	40% < X < 50%	50% < X < 60%	60% < X < 70%	70% < X < 80%	80% < X < 90%	90% < X < 100%	100%
[300–212]	MLA	501 (100%)	17 (3.4%)	6 (1.2%)	20 (4.0%)	63 (12.6%)	50 (10%)	62 (12.4%)	43 (8.6%)	42 (8.4%)	39 (7.8%)	29 (5.8%)	22 (4.4%)	108 (21.6%)
	OptLib	504 (100%)	20 (4.0%)	4 (0.8%)	23 (4.6%)	56 (11.1%)	47 (9.3%)	54 (10.7%)	46 (9.1%)	45 (8.9%)	35 (6.9%)	34 (6.7%)	20 (4.0%)	120 (23.8%)
[212–150]	MLA	596 (100%)	53 (8.9%)	8 (1.3%)	27 (4.5%)	34 (5.7%)	49 (8.2%)	43 (7.2%)	36 (6.0%)	47 (7.9%)	39 (6.5%)	38 (6.4%)	27 (4.5%)	195 (32.7%)
	OptLib	561 (100%)	45 (8.0%)	9 (1.6%)	22 (3.9%)	29 (5.2%)	41 (7.3%)	38 (6.8%)	30 (5.3%)	42 (7.5%)	37 (6.6%)	39 (7.0%)	28 (5.0%)	201 (35.8%)
[150–106]	MLA	768 (100%)	146 (19.0%)	11 (1.4%)	33 (4.3%)	36 (4.7%)	34 (4.4%)	47 (6.1%)	39 (5.1%)	37 (4.8%)	59 (7.7%)	53 (6.9%)	33 (4.3%)	240 (31.3%)
	OptLib	760 (100%)	138 (18.2%)	9 (1.2%)	28 (3.7%)	33 (4.3%)	30 (3.9%)	43 (5.7%)	40 (5.3%)	38 (5.0%)	55 (7.2%)	55 (7.3%)	35 (4.6%)	256 (33.7%)

magnetite. Based on the X-ray analysis, a qualitative evaluation indicated that quartz and goethite were present in higher concentrations than hematite and magnetite. Regarding the iron oxide minerals hematite and magnetite, hematite was present in higher concentration than magnetite. The *Opt*$_{-Lib}$ and *MLA* analytical data for the mineral phase quantification (modal analyses) performed on the same iron ore sample for the 300–212-μm, 212–150-μm, and 150–106-μm size classes are presented in Fig. 9 and also in Table 2.

The results of the mineral phase quantifications for the three analysed size classes produced by both systems are very similar and in accordance with the qualitative results obtained from the X-ray analysis. The observed differences were expected and most likely result from the built-in technological differences within each system.

A real validation of these results based on X-ray diffraction applying Rietveld Refinement Methodology (RRM) is under development.

The total number of particles analysed by each system varied from 1150 to 1250 in each class size. This provides a very good statistical confidence. For the quartz and goethite minerals, both systems exhibit similar results, which means that the *Opt*$_{-Lib}$ system accomplished the expected task of distinguishing quartz from epoxy resin. Regarding the quantification of the hematite and magnetite minerals, it is also evident that the *MLA* (contrary to the *Opt*$_{-Lib}$) was not capable of recognizing them as distinct mineral phases; instead, they are both designated as hematite in Fig. 9 and Table 2. For all size classes, the summations of the values obtained for magnetite and hematite using the *Opt*$_{-Lib}$ system are very similar to the hematite values given by the *MLA* analysis.

3.5.2. Iron ore liberation analysis

The three size classes examined in the mineral phase quantification study were also used in the liberation analysis involving both digital image analysis systems. For each size class, the number of sampled images was sufficiently large to guarantee that a minimum of 500 particles from each class was analysed by each system.

In the liberation analysis, goethite, hematite, and magnetite were grouped together and considered to be a single mineral phase. These mineral phases were denominated "iron oxides", and the liberation analysis of the iron oxides as a group was conducted relative to quartz. Table 3 correlates particle surface distribution by areal composition with the respective particle distribution by composition classes. Thus, the same procedure was adopted for classifying the particles surface area in classes of areal composition for both systems MLA and *Opt*$_{-Lib}$. So they can be compared. The areal composition were distributes in 12 classes where 0% represents pure gangue minerals and 100% represents pure mineral particles. From 0% to 100% 10 intermediated classes of areal composition were set.

Fig. 10 shows the distribution function of the cumulative particle percentage content classified according to composition. The particle composition is distributed perceptually from 0 to 100 in 12 composition classes. The graphs in Fig. 10 show, for each size class, the cumulative percentages of particles with composition greater than a certain value (the class range). Note that these computations consider only particles with compositions in iron oxide greater than zero.

The results show that, for each size class, the percentage of liberated iron oxide particles, as calculated by the *MLA* system, was very close to that yielded by the *Opt*$_{-Lib}$ system. Considering, for instance, the 300–212-μm size class, the percentage of liberated iron oxide particles was approximately 22%, according to the *MLA* system. This can be compared to the approximate value of 25% given by the *Opt*$_{-Lib}$ system. Considering another point on the

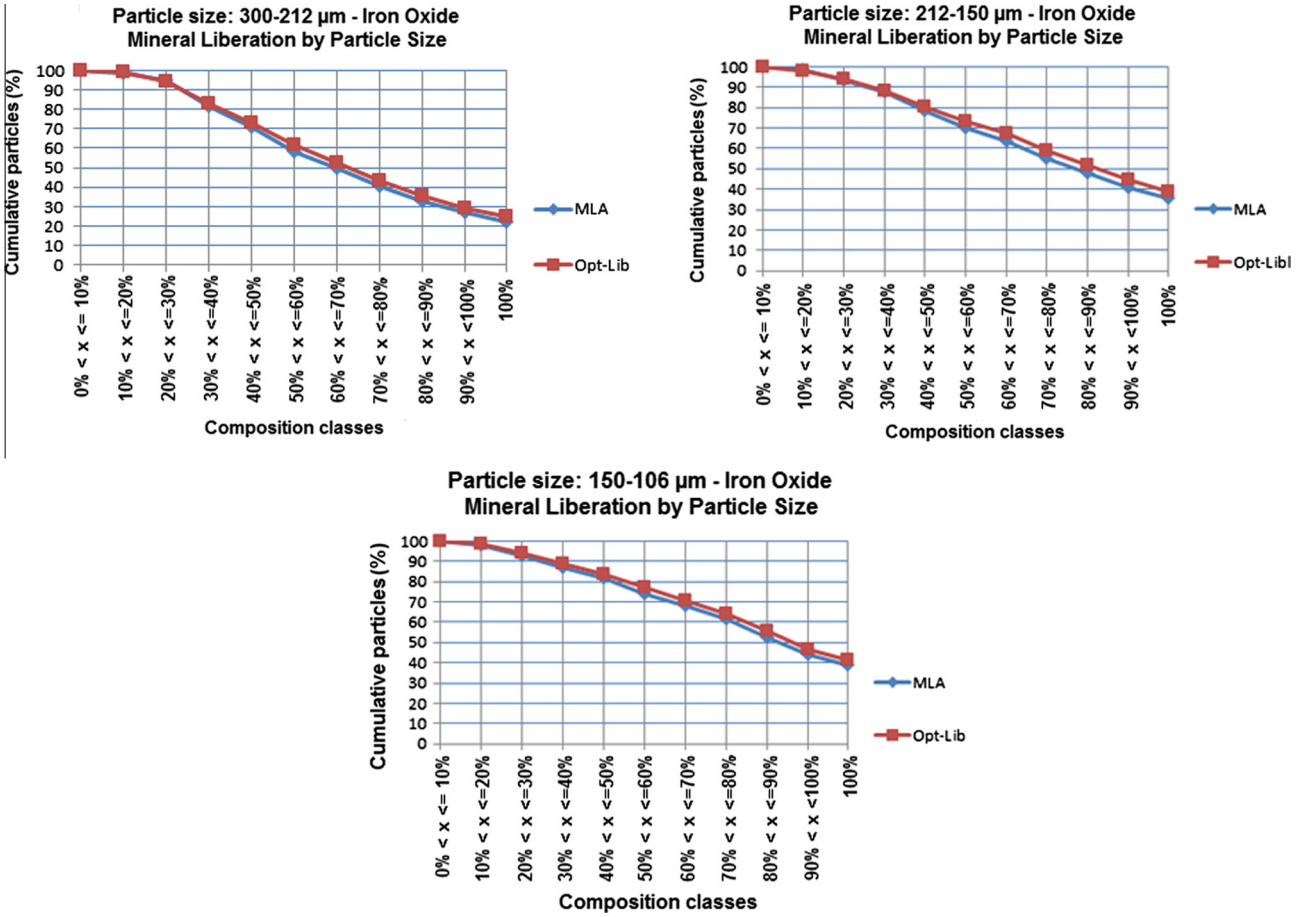

Fig. 10. Cumulative particle composition distribution obtained from *MLA* and *Opt*$_{-Lib}$ for the size classes: 300–212, 212–150, and 150–106 µm.

same curve, for instance, the class representing particles with composition greater than 50% in iron oxide, both systems exhibit values close to 60%. The same trends are observed for the other size classes analysed here, i.e., 212–150 and 150–106 µm.

From the results for the three examined size classes presented in Table 3 and Fig. 10, it can be concluded that the liberation analysis performed using both the *MLA* and *Opt*$_{-Lib}$ systems yielded very similar results. The slight differences can be attributed to factors such as:

- the initial parameter configurations of each system;
- differences in the particle population analysed by one system that may not necessarily have been identical to that analysed by the other system;
- different segmentation techniques.

4. Conclusions

A digital image analysis system was developed to perform mineralogical characterisation and liberation analysis of iron ores, based on the analysis of digital images obtained using a reflected light optical microscope (RLOM). The system increased the analytical precision of the RLOM technique as regards the assessment of mineral phases such as quartz, goethite, hematite, and magnetite. The technique applied an intensive sampling preparation and polishing methodology to overcome a classical problem encountered during the analysis of digital images taken from a RLOM: classification of the quartz mineral as a different phase to the epoxy resin and discrimination between them. Once the quartz/epoxy resin problem was overcome and, considering the fact that RLOM also allows discrimination between magnetite and hematite, it was possible to perform a modal analysis of the iron ore samples. A performance evaluation was conducted in which the *Opt*$_{-Lib}$ and Mineral Liberation Analyzer (*MLA*) systems were compared. Samples of a Brazilian iron ore containing three particle size classes (300–212, 212–150, and 150–106 µm) were subjected to analysis using both systems. The differences observed in the obtained results were not significant and can be attributed to characteristic factors of each system. The results obtained for the modal analyses are indicative that the quartz/epoxy resin discrimination problem has been satisfactorily solved for the RLOM system. Further, the *Opt*$_{-Lib}$ system has an advantage in that it can classify hematite and magnetite as different mineral phases. The *Opt*$_{-Lib}$ methodology can result in a promising iron ore characterisation system if adapted to recognize the different hematite characteristics such as the lamellar, granular and recrystallized ones.

Acknowledgements

The authors would like to thank the Brazilian agencies PROEX-CAPES, CNPq, and FAPEMIG for funding this research.

References

Barbery, G., 1992. Liberation 1, 2, 3: theoretical analysis of the effect of space dimension on mineral liberation by size reduction. Miner. Eng. 5 (2), 123–141.

Chescoe, D.C., Goodhew, P.J., 1990. The Operation of Transmission and Scanning Electron Microscopes, Microscopy Handbook, first ed. Oxford University Press, Oxford, p. 20.

Delbem, I.D., 2010. Digital Image Analysis and Processing Applied to Mineral Liberation Studies, (in Portuguese). Master Degree, Mineral Technology, PPGEM, Escola de Engenharia, Universidade Federal de Minas Gerais, Belo Horizonte, p. 99.

Delbem, I.D., 2014. Automated Iron Ores Characterisation via Reflected Light Optical Microscope, (in Portuguese). Doctoral Thesis in Mineral Technology, PPGEM, Escola de Engenharia, Universidade Federal de Minas Gerais, Belo Horizonte, p. 122.

Diday, E., Moreau, J.V., 1984. Learning hierarchical clustering from examples – application to the adaptive construction of dissimilarity indices. Pattern Recogn. Lett. 2, 365–378.

Donskoi, E., Suthers, S.P., Fradd, S.B., Young, J.M., Campbell, J.J., Raynlyn, T.D., Clout, J.M.F., 2007. Utilization of optical image analysis and automatic texture classification for iron ore particle characterization. Miner. Eng. 20, 461–471.

Donskoi, E., Poliakov, A., Manuel, R.J., Raynlyn, T.D., 2010. Advances in optical image analysis and textural classification of iron ore fines. In: 25th International Mineral Processing Congress, Brisbane, pp. 2823–2836.

Donskoi, E., Poliakov, A., Manuel, J.R., Peterson, M., Hapugoda, S., 2013a. Industrial strength optical image analysis system – Mineral4/Recognition4. In: Proceedings Iron ore, Perth, pp. 227–241.

Donskoi, E., Manuel, J.R., Austin, P., Poliakov, A., Peterson, M.J., Hapugoda, S., 2013b. Comparative study of iron ore characterization using a scanning electron microscope and optical image analysis. Trans. Inst. Min. Metal. B 122 (4), 217–229.

Dunham, S., Vann, J., 2007. Geometallurgy, Geostatistics and Project Value – Does Your Block Model Tell You What You Need to Know? Project Evaluation Conference, Melbourne, Victoria, 19–20 June, pp. 1–8.

Fandrich, R., Gu, Y., Burrows, D., Moeller, K., 2007. Modern SEM-based mineral liberation analysis. Int. J. Miner. Process. 84, 310–320.

Gonzalez, R.C., Woods, R.E., 2008. Digital Image Processing, third ed. Prentice Hall, New Jersey, p. 624.

Goodall, W.R., Scales, J.J., Butcher, A., 2005. The use of QEMSCAN and diagnostic leaching in the characterisation of visible gold in complex ores. Miner. Eng. 18 (8), 877–886.

Gu, Y., Napier-Munn, T., 1997. JK/Phylips Mineral Liberation Analyzer – An Introduction, Mineral Processing'97, Conf., Cape Town, SA, p. 2.

Iglesias, J.C.A., Gomes, O.F.M., Paciornick, S., 2011. Automatic recognition of hematite grains under polarized reflected light microscopy through image analysis. Miner. Eng. 24, 1264–1270.

King, R.P., 1984. Measurement of particles size distribution by image analyser. Powder Technol. 39, 279–289.

Launeau, P., Cruden, A.R., Bouchez, J.L., 1994. Mineral recognition in digital images of rocks: a new approach using multichannel classification. Can. Mineral. 32, 919–933.

Lin, C.L., Hsieh, Chiang-Hao, Tserendagva, Tsend-Ayush, Miller, J.D., 2013. Dual energy rapid scan radiography for geometallurgy evaluation and isolation of trace mineral particles. Miner. Eng. 40, 30–37.

Neumann, R., Stanley, C.J., 2008. Specular reflectance data for quartz and some epoxy resins – implications for digital image analysis based on reflected light optical microscopy. In: ICAM 2008, Brisbane, pp. 703–705.

Pirard, E., 2004. Multispectral imaging of ore minerals in optical microscopy. Mineral. Mag. 68 (2), 323–333.

Pirard, E., Lebichot, S., Krier, W., 2007. Particle texture analysis using polarized light imaging and grey level intercepts. Int. J. Miner. Process. 84, 299–309.

Poliakov, A., Donskoi, E., 2014. Automated relief-based discrimination of non-opaque minerals in optical image analysis. Miner. Eng. 55, 111–124.

Schneider, C.L., 1995. Measurement and Calculation of Liberation in Continuous Milling Circuits, 1995, PhD, thesis, University of Utah.

Shutherland, D., 2007. Estimation of mineral grain size using automated mineralogy. Miner. Eng. 20, 452–460.

Tonzetic, I., Dippenaar, A., 2011. An alternative to traditional iron-ore sinter phase classification. Miner. Eng. 24, 1258–1263.

Wahlstrom, E.E., 1969. Optical Crystallography, third ed. Ao Livro Técnico, São Paulo.